



Figure 2 shows an intensity map calculated in the coordinates $(2\theta; \theta_i)$, assuming $\theta_f = 0,5^\circ$ where 2θ is the in-plane scattering angle. In this map, a part of the Debye ring of Nb110 and Al220 is depicted. The width of the ring in the 2θ direction is inversely proportional to the grain radius R . Along the Debye ring, the intensity modulation follows the dependence of the intensity of the wave-field on θ_i ; the period of the modulation is inversely proportional to the multi-layer period. The rings Nb110 and Al220 have different structures; these differences are caused by different intensities of the standing wave in Nb and Al layers. Below θ_c , the penetration depth of the incoming beam is very small and no diffraction from the grains takes place.

Figure 3 shows the intensity scans for $2\theta = \text{const.}$ calculated for Nb110 and Al220 diffraction and reflection on assuming multi-layer.

IV. Conclusions

Model with flat interfaces (and expectations in paragraph III.) is too simplified to describe real experimental data. The most important point of the further work is description of the scattering process from interfaces roughness. The next problems are the texture, influence of the random size of the grains, etc.

References

- [1] S.K. Sinha, E.B. Sirota, S. Garoff, and H.B. Stanley, *Phys. Rev. B* **38**, 2297 (1988).
- [2] V. Holý, U. Pietsch, and T. Baumbach, *High Resolution X-Ray Scattering from Thin Films and Multilayers*, (Springer, Berlin 1999).

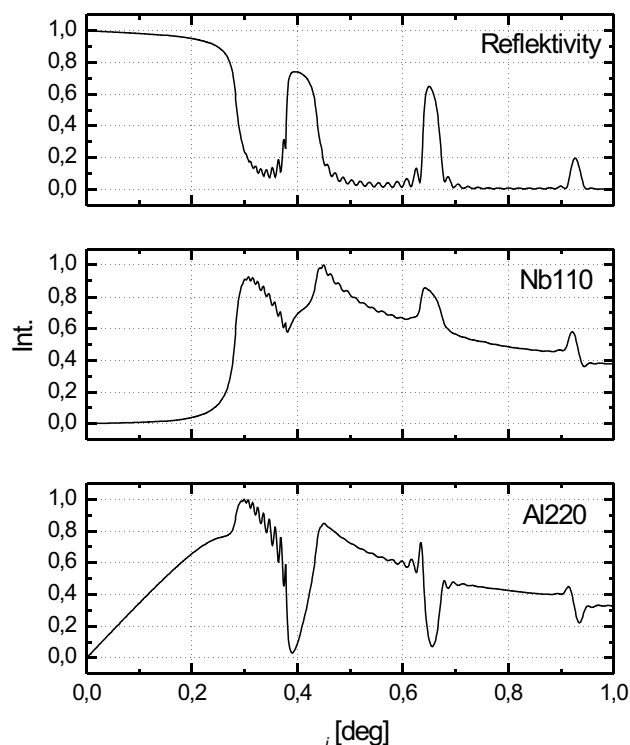


Fig.3. The intensity scans for $2\theta = \text{const.}$ for Nb110 and Al220 and reflection on multi-layer, mean grain size $R = 2 \text{ nm}$, $\theta_f = 0,5^\circ$.

TANTALONIOBATES IN CASSITERITE: INCLUSIONS OR EXSOLUTIONS?

M. Klementová^{1,2}, M. Rieder³

¹*Institute of Inorganic Chemistry, Academy of Sciences of the Czech Republic*

²*IGMMR, Faculty of Science, Charles University in Prague, Czech Republic*

³*Institute of Materials Chemistry, VŠB – Technical University of Ostrava*

Keywords

Tantaloniobates, cassiterite, exsolution process, inclusion, pegmatite

Abstract

Tantaloniobates in cassiterite from the Annie-Claim Pegmatite (Canada) and pegmatites in the Czech Massif were studied by the following methods: light microscopy, single-crystal X-ray diffraction, electron microprobe, and transmission electron microscopy (TEM). A concentration gradient around inclusions (electron microprobe results) and a defined structural orientation of inclusions within the cassiterite matrix (X-ray and electron diffraction results) were observed. This confirms that in the cases studied, tantaloniobates in cassiterite formed as a result of an exsolution process.

Introduction

In natural samples, it is sometimes difficult to differentiate between inclusions that were trapped during crystal growth and products of post-crystallization exsolution processes. In order to understand the process of rock formation, the inclusions/exsolution have to be studied in detail. Presently, we studied cassiterite from the Annie-Claim Pegmatite (Canada) and pegmatites in the Czech Massif. The following methods were employed: light microscopy, single-crystal X-ray diffraction, electron microprobe and transmission electron microscopy (TEM).

The word “inclusion” is being used loosely. In general, an inclusion can be any solid or fluid phase enclosed in the surrounding matrix. This covers inclusions *sensu stricto*, which are randomly trapped by a crystal during its growth, as well as precipitates that form by exsolution in the subsolidus. Hereafter, we shall use the term “inclusion” in non-genetic context, whereas the term “inclusion *sensu stricto*” as opposed to terms “precipitate” or “exsolution” will allude to the formation process involved.

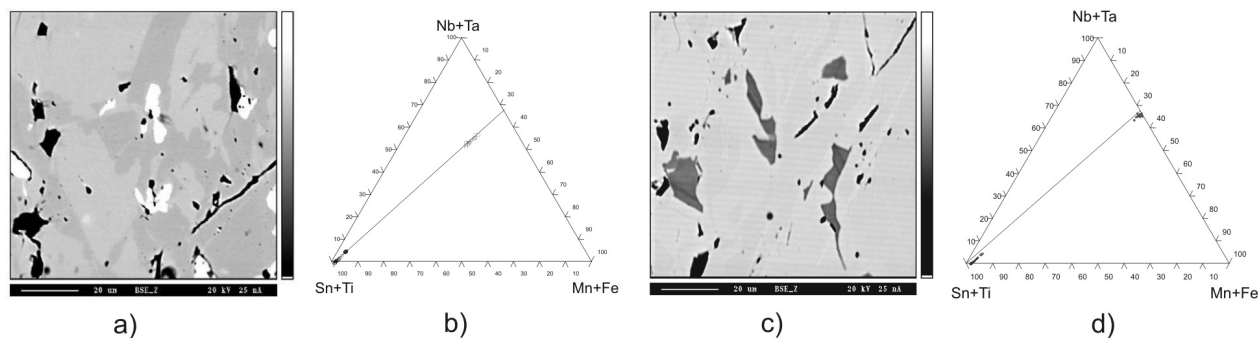


Figure 1. a) Sample from Annie Claim 3 in back-scattered electrons (BSE). White - wodginite inclusions, light grey - enriched cassiterite, dark grey - depleted cassiterite. b) Microprobe analyses of sample 206-IVA from Annie Claim 3 plotted in triangular diagram Sn+Ti - Mn+Fe - Nb+Ta (at.%). c) Sample from Nová Ves in back-scattered electrons (BSE). White - columbite inclusions, light grey - depleted cassiterite, enriched grey - depleted cassiterite. d) Microprobe analyses of sample MM-116 from Nová Ves plotted in triangular diagram Sn+Ti - Mn+Fe - Nb+Ta (at.%).

There are several ways how to differentiate between inclusions *sensu stricto* and precipitates. Under the microscope, a first impression comes from the shape and spatial distribution of inclusions within the matrix. Inclusions *sensu stricto* usually are irregular in shape and are distributed randomly, whereas precipitates form lamellae or assume other distinct shapes and tend to be arranged in preferred directions, as demanded by their structural orientation within the host. In the matrix surrounding a precipitate, a concentration gradient may betray that a diffusion of elements toward the precipitate took place during its growth; contrariwise, the matrix around an inclusion *sensu stricto* ought to be homogeneous. To obtain yet another piece of evidence, one might want to perform a single-crystal diffraction experiment in order to see whether a precipitate is crystallographically aligned in the host. The underlying idea is that there are hardly any compelling reasons to expect inclusions *sensu stricto* to assume a fixed crystallographic orientation with respect to the matrix.

Tantaloniobates such as ixiolite and columbite have commonly been described as inclusions or precipitates (exsolution products) in cassiterite and rutile [1, 2, 3, 4, 5, 6, 7, 8, 9, 10, 11]. However, these studies relied on reflected-light microscopy, microprobe analyses, and X-ray powder diffraction, which may not suffice to differentiate unequivocally between inclusions *sensu stricto* and exsolution products.

Chemical composition

Texture and chemical composition were studied with the help of electron microscopy (SEM and microprobe). Selected samples were analyzed quantitatively on the microprobe Cameca SX50 with a Wave Dispersive Spectrometer (operated at 20kV, 25nA) at the NHM in London. All analyses were recalculated on the basis of 24 oxygens to allow an easy comparison among all phases involved.

In the material studied, it is possible to discern two groups of samples, in agreement with their locality as well as their chemical composition. Canadian samples contain precipitates of monoclinic wodginite $MnSnTa_2O_8$, whereas samples from the Czech Massif contain orthorhombic ferrocolumbite $Fe(Nb,Ta)_2O_6$. In the samples from both groups, a concentration gradient surrounding the inclusions can be observed (Fig. 1).

Canadian cassiterite contains inclusions of wodginite $SnMnTa_2O_8$, which appear lighter than surrounding cassiterite in back-scattered electrons (fig. 1a). In BSE, the concentration gradient in cassiterite matrix in the vicinity of inclusions is visible. The dark zones surrounding inclusions are composed of pure cassiterite - “depleted” cassiterite (depleted in comparison with primary cassiterite, which is enriched in minor elements), whereas the lighter areas farther from the inclusions and inclusion-free are primary “enriched” cassiterite with higher concentration of Ta, Mn, Nb and Fe (tab 1).

Chemical composition of the inclusions corresponds to wodginite $SnMnTa_2O_6$. The major substitutions are homovalent such as Fe-Mn, Nb-Ta a Zr-Sn. Inclusions concentrate Ti, Sc, Mn, Ta and Zr, while cassiterite prefers Fe and Nb. In figure 1b, analyses from sample 206-IVA from Annie Claim 3 are plotted in the triangular diagram Sn+Ti - Mn+Fe - Nb+Ta (at. %). It is shown that the analyses of enriched and depleted cassiterite cluster in two areas, which are separated by 5% $(Mn,Fe)(Ta,Nb)_2$ component. All analyses fall on the same line that connects the Sn+Ti apex with $(Mn,Fe)(Ta,Nb)_2$. Such pattern is usually attributed to magma mixing (in case of rocks) or unmixing (this case).

Chemical composition of the inclusions in cassiterite from the Czech Massif corresponds to columbite $Fe(Nb,Ta)_2O_6$. Figure 1c shows cassiterite from Nova Ves in back-scattered electrons. A concentration gradient surrounding inclusion is visible, even though it is much weaker than in the case of samples containing wodginite. In this case, inclusions appear darker than the matrix. The reversed contrast is due to the average molecular weight of inclusions, which is lower than that of cassiterite, whereas in the samples from Annie Claim 3 the inclusions are “heavier” than the matrix. Quantitative analyses are listed in table 1.

The major substitutions active here are homovalent such as Fe-Mn and Nb-Ta. Inclusions concentrate Ti and Nb, while cassiterite prefers Ta. In figure 1d, analyses from sample MM-116 from Nova Ves are plotted in the triangular diagram Sn+Ti - Mn+Fe - Nb+Ta (at.%). Also in this case the analyses fall on the same line, which connects the Sn+Ti apex with $(Mn,Fe)(Ta,Nb)_2$.



Table 1.: Microprobe analyses of samples 206-IVA from Annie Claim 3 and MM-116 from Nová Ves.. Calculation is based on 24O. (IN – inclusion, DC – depleted cassiterite, EC – enriched cassiterite).

	Annie Claim			Nova Ves		
	IN	DC	EC	IN	DC	EC
Ti	0.025	0.000	0.000	0.151	0.015	0.010
Na	0.012	0.084	0.059	0.000	0.069	0.044
Ca	0.000	0.000	0.000	0.010	0.000	0.000
Sc	0.036	0.000	0.001	0.011	0.000	0.003
Sn	2.274	11.928	11.059	0.089	11.786	11.157
Mn	2.737	0.004	0.224	0.333	0.005	0.013
Fe	0.225	0.006	0.031	3.334	0.024	0.232
Zr	0.402	0.012	0.042	0.086	0.051	0.034
Nb	0.795	0.005	0.091	6.134	0.024	0.366
Ta	5.367	0.018	0.506	1.693	0.050	0.150
Y	-	-	-	0.000	0.002	0.000
Th	-	-	-	0.013	0.005	0.000
U	-	-	-	0.012	0.000	0.010
Sb	-	-	-	0.002	0.016	0.006
Hf	0.077	0.006	0.008	0.010	0.006	0.004
W	0.006	0.000	0.000	0.005	0.000	0.000
Bi	-	-	-	0.000	0.000	0.000
Total	11.956	12.062	12.022	11.883	12.052	12.029

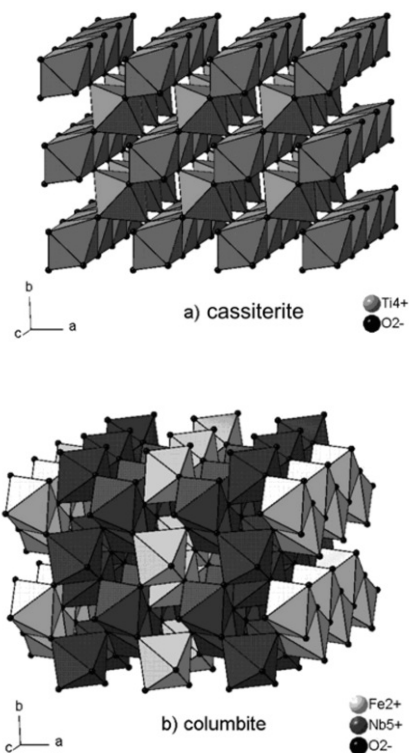


Figure 2.: Structure of cassiterite (a) and columbite (b).

Structural orientation

Cassiterite, SnO_2 , belongs to the rutile structural group whose members crystallize in space group $P4_2/mnm$. Cell parameters of synthetic SnO_2 are: $a = 4.738 \text{ \AA}$, $c = 3.186 \text{ \AA}$ [12]. Its structure consists of edge-sharing SnO_6 octahedra that form chains along the c axis and are interconnected in the $[110]$ direction by means of apices of octahedra (fig. 2a).

Tantaloniobates such as ixiolite, columbite-tantalite and wodginite, occurring as inclusions in cassiterite have related structures. All these structures can be described as zig-zag chains of octahedra extending parallel to the c axis (fig. 2b). Individual structures differ by the kind of octahedral cations and their ordering. The structural relationships can be summarized as follows [13]. The common unit is the cell of ixiolite. Ordered columbite-tantalite has unit cell parameters $a = 3a_{ix}$, $b = b_{ix}$, $c = c_{ix}$ and ordered wodginite $a = 2a_{ix}$, $b = 2b_{ix}$, $c = c_{ix}$. Therefore, we can expect all these tantaloniobates to assume a similar orientation within the structure of cassiterite.

Structural orientation of tantaloniobate inclusions in cassiterite was studied by means of single-crystal X-ray diffraction and transmission electron microscopy.

X-ray diffraction

The spatial relation of tantaloniobate precipitates within the host cassiterite predicted by a close examination of their structures was confirmed by single-crystal X-ray diffraction. An Enraf-Nonius precession camera with unfiltered MoK ($\lambda = 0.7107 \text{ \AA}$) radiation was used. In order to observe diffraction spots of lamellae which represent a small fraction of the volume of host cassiterite, overexposed photographs had to be taken, further boosted with an intensifier screen. Where continuous radiation hampered the interpretation of photographs, the radiation was Zr-filtered.

Mutual crystallographic orientation of the lattices of cassiterite and tantaloniobate exsolutions (either ferrocolumbite or wodginite) is as follows (fig. 3): the reciprocal axis c^* of each precipitate is approximately parallel to one of the cassiterite directions $[101]^*$, $[011]^*$, $[10\bar{1}]^*$, $[0\bar{1}1]^*$. The precipitates' a^* axes are strictly parallel to the a_1^* and a_2^* axes of cassiterite, whereas b_{col}^* is not parallel to any rational reciprocal direction of cassiterite.

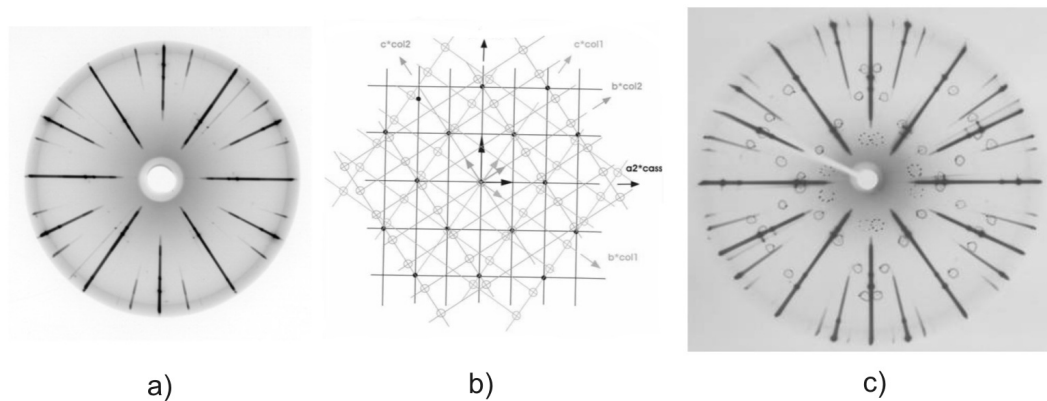


Figure 3: Precipitates of tantaloniobates in cassiterite. (a) precession photograph of $0kl^*$ net of cassiterite with $0kl^*$ net of ferrocolumbite (sample MM-116 from Nova Ves - Czech Republic), (b) interpretation, (c) precession photograph of $0kl^*$ net of cassiterite with $0kl^*$ net of wodginite (sample 206-IVA-d from Annie Claim pegmatite - Canada).

Generally, there are four possible orientations of tantaloniobate precipitates, dictated by the tetragonal symmetry of cassiterite. However, in the crystal from Nova Ves only one orientation was observed (corresponding to col_2 in the figure 3b), whereas in sample from Annie-Claim pegmatite at least two different orientations can be observed (fig. 3c).

Electron diffraction

Size, morphology and arrangement of precipitates and characteristics of interface between host cassiterite and individual precipitates were studied in TEM at the Johns Hopkins University (Baltimore, MD, USA).

Samples were prepared from thin sections by placing Cu-grids on selected areas of interest and ion-milled to the TEM thickness by Ar-ions. Two instruments were used - Philips EM420 at 120 kV and Philips CM300 at 300 kV (FEG), both equipped with an EDS detector. Digital images were treated with Digital Micrograph, and simulation of electron diffraction patterns was produced in MacTempas. EDS analysis were obtained and processed with DTSA and EmiSpec software.

In the TEM (fig. 4a,c), inclusions ranging from 0.1 μ m to 1 μ m were observed; no finer scale exsolution products were detected. Chemical composition of the inclusions is the same as analyzed on the microprobe and corresponds to wodginite and ferrocolumbite, respectively.

Structural orientation of the inclusions towards the cassiterite matrix at the interface was examined on about 40 inclusions by means of electron diffraction. The orientation of all the inclusions confirms the results of X-ray diffraction. However, a slight misorientation of several degrees was established.

Examples of inclusions from both localities are shown in figure 4. It can be seen that the reciprocal direction $[100]^*$ of cassiterite coincides with the $[100]^*$ of inclusions (wodginite or ferrocolumbite). The other parallel directions are: in the sample from Annie Claim $[201]^*$ of cassiterite with $[010]^*$ of wodginite (fig. 4b) and in the sample from the Czech Massif $[021]^*$ of columbite with $[100]^*$ of cassiterite (fig. 4d). These relations correspond to the ori-

entation relationships determined by X-ray diffraction (fig. 3b).

Conclusions

In the samples of cassiterite from the Annie-Claim Pegmatite (Canada) and pegmatites in the Czech Massif, a concentration gradient around inclusions (electron microprobe results) and a defined structural orientation of inclusions within the cassiterite matrix (X-ray and electron diffraction results) was observed. This confirms that in the cases studied, tantaloniobates in cassiterite formed as a result of an exsolution process.

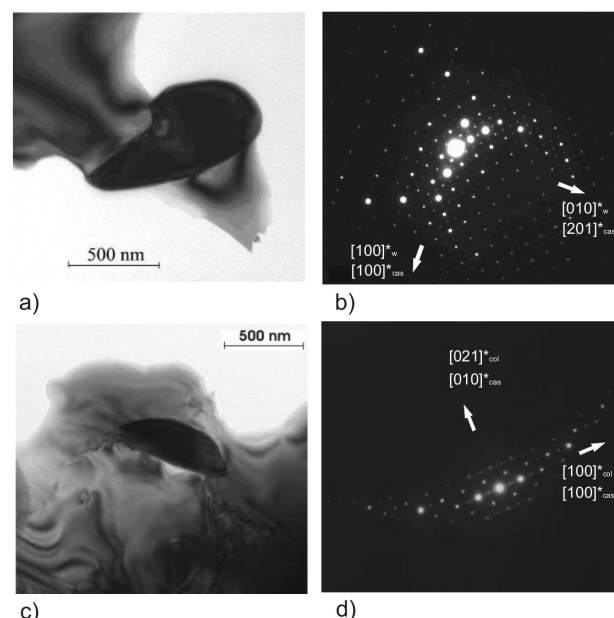


Figure 4. TEM observations. (a) wodginite inclusion in cassiterite (sample 222a Annie-Claim pegmatite), (b) corresponding electron diffraction, (c) ferrocolumbite inclusion in cassiterite (sample MM-97 the Czech Massif), (d) corresponding electron diffraction.



The mechanism utilized during exsolution of tantaloniobate precipitates in cassiterite is nucleation and growth (not spinodal decomposition – see [14] for description of both mechanisms). The precipitates are in the late stage of exsolution characterized by advanced coarsening and a slight rotation of the phase boundaries. Even though pegmatites are considered to be highly dis-equilibrated and fast cooling rocks [15,16] it seems that at least at some level equilibrium is close to being achieved.

Tantaloniobate precipitates were found in cassiterite with elevated concentrations of Ta as well as Nb. In contrast, tantaloniobate exsolution products found in rutile (isostructural with cassiterite) are restricted to samples rich in Nb; Ta-rutile appears to be a homogeneous solid solution resistant to exsolution [1,2,4,6,7,8].

We should like to thank Prof. Petr Černý (University of Manitoba, Canada) and Prof Milan Novák (Masaryk University, Czech Republic) for making available the samples for this study. The study was supported by the following grants: the Grant Agency of Charles University (grant No. 198/2000 B GEO), the Grant Agency of the Czech Republic (grant No. 205/01/1126). The electron microprobe analyses were collected during the senior author's stay at the Natural History Museum (London) under the SYS-RESOURCE program. The transmission electron microscopy studies were conducted at the Johns Hopkins University (Baltimore, MD) under the supervision of Prof. David Veblen and were sponsored by the NSF grant and Fulbright scholarship.

References

1. P. Černý, F. Čech & P. Povondra, *Neues Jb. Miner. Abh.* 101(2) (1964), 142-172.
2. P. Černý, B.J. Paul, F.C. Hawthorne & R. Chapman, *Can. Mineral.* 19 (1981), 541-548.
3. P. Černý, W.L. Roberts, T.S. Ercit & R. Chapman, *Am. Mineral.* 70 (1985), 1044-1049.
4. P. Černý, R. Chapman, R. Goad, G. Niedermayer & M.A. Wise, *Mineral. Petrol.* 40.(1989), 197-206.
5. P. Černý, T.S. Ercit, M.A. Wise, R. Chapman & H.M. Buck, *Can. Mineral.* 36 (1998), 547-561.
6. P. Černý, R. Chapman, W.B. Simmons & L.E. Chackowsky, *Am. Mineral.* 84 (1999), 754-763.
7. P. Černý, R. Chapman & M. Masau, *Can. Mineral.* 38 (2000), 907-913.
8. P. Černý, M. Novák, R. Chapman & M. Masau, *J. Czech Geol. Soc.* 45/1 (2000), 21-35.
9. M. Masau, P. Černý & R. Chapman, *Can. Miner.* 38 (2000), 685-694.
10. A.M.R. Neiva. *Can. Mineral.* 34 (1996), 745-768.
11. A.G. Tindle, F.W. Breaks & P.C. Webb, *Can. Mineral.* 36 (1998), 637-658.
12. H. Seki, N. Ishizawa, N. Mizutani & M. Kato, *J. Ceram. Soc. Jpn.* 92 (1984), 219-223.
13. J.D. Grice, R.B. Ferguson. & F.C. Hawthorne, *Can. Mineral.* 14 (1976), 540-549.
14. A. Putnis: Introduction to Mineral Sciences. Cambridge University Press 1992.
15. P. Černý, *Geoscience Canada* 18 (1991), 2, 49-67.
16. P. Černý, *Geoscience Canada* 18 (1991), 2, 68-81.

